Depth-Dependent Dissociation of Nitric Acid at an Aqueous Surface: Car−Parrinello Molecular Dynamics

Shuzhi Wang,[†] Roberto Bianco,*[,†] and James T. Hynes*[,†,‡,§]

Department of Chemistry and Biochemistry, University of Colorado, Boulder, Colorado 80309-0215, USA, Ecole Normale Supérieure, Chemistry Department, 24 rue Lhomond 75005 Paris, France, and CNRS UMR Pasteur

Received: September 25, 2008; Revised Manuscript Received: December 3, 2008

The acid dissociation of a nitric acid HNO_3 molecule located at various depths in a water slab is investigated via Car−Parrinello molecular dynamics simulations. HNO_3 is found to remain molecular when it is adsorbed on top of the surface with two hydrogen-bonds, and to dissociate—although not always—by transferring a proton to a water molecule within a few picoseconds when embedded at various depths within the aqueous layer. The acid dissociation events are analyzed and discussed in terms of the proton donor−acceptor O−O hydrogen bonding distance and the configurations of the nearest-neighbor solvent waters of an $HNO_3 \cdot H_2O$ pair. Four key structural features for the HNO_3 acid dissociation are identified and employed to analyze the trajectory results. Key solvent motions for the dissociation include the decrease of the proton donor−acceptor O−O hydrogen bonding distance and a 4 to 3 coordination number change for the proton-accepting water. The Eigen cation (H_3O^+), rather than the Zundel cation ($H_5O_2^+$), is found to be predominant next to the NO_3^- ion in contact ion pairs in all cases.

1. Introduction

In the present work, we continue our theoretical investigation of the acid dissociation of nitric acid HNO_3[1,2]

$$HNO_3 + H_2O \rightarrow NO_3^- + H_3O^+ \quad (1)$$

at an aqueous surface. Our work[1] as well as other theoretical[3] and experimental[4−12] efforts suggest that the proton transfer (PT) eq 1 may not occur on and in the uppermost portions of an aqueous surface despite the fact that HNO_3 is a well-known strong acid in bulk aqueous solutions.[13] Here we address the following questions: At what depth into an aqueous sample does the acid dissociation occur? And what are the key molecular level aspects promoting that dissociation? As in refs 1 and 2, our focus is on HNO_3 under "infinitely" dilute conditions, motivated by our special interest in the uptake of HNO_3 on the aqueous surface of cirrus cloud particles in the upper troposphere; here uptake involves a $\leq$0.1 effective monolayer coverage of HNO_3, where the dissociation state has not been determined experimentally.[14,15]

In fact, nitric acid is important in heterogeneous chemistry in various atmospheric contexts. Nitrate aerosols (mainly nitric acid trihydrate) can serve as one site for stratospheric heterogeneous reactions whose products in turn lead to stratospheric ozone depletion.[16] HNO_3 is also a product of many of these reactions, such as the key reaction of chlorine nitrate with hydrochloric acid on water ice aerosols.[16,17] In the troposphere, many uptake processes and heterogeneous reactions involve HNO_3.[14,15,18−27] For example, "renoxification", a heterogeneous reaction of molecular HNO_3 with NO, produces reactive nitrogen oxides significant in tropospheric pollution.[18] In the marine troposphere, HNO_3 uptake on sea salt aerosols is an important NO_x removal process.[19] In the upper troposphere, where water ice aerosols are abundant in cirrus clouds, HNO_3 uptake on water/ice aerosols (mentioned above) plays an important role in determining ozone concentration. HNO_3 can also lead to NO_2 formation which ultimately produces ozone and can be removed (sequestered) by water/ice aerosols.[20] The HNO_3 coated water/ice aerosols can significantly hinder heterogeneous chlorine chemistry, such as chlorine nitrate's hydrolysis or its reaction with hydrochloric acid.[21−23]

The acid ionization state of HNO_3 at an aqueous surface is the key to the understanding of the mechanisms of many of these processes. For example, it could be expected to assist in the uptake of HNO_3 by cirrus cloud surfaces.[1,2,14,15,24,25] Further, the presence of molecular HNO_3 or its acid dissociation product NO_3^- ion at an aqueous aerosol surface implies different reaction mechanisms; an extreme example is the renoxification reaction mentioned above, which requires molecular, rather than dissociated, HNO_3.[18]

HNO_3 acid dissociation at an aqueous surface also has important fundamental significance. As noted above, HNO_3 is usually regarded as a strong acid, in view of its behavior in dilute aqueous solutions[13] (although not at high concentrations[28,29]). But at the surface there is less solvation, and the ease of the dissociation eq 1 is not at all self-evident, and as mentioned above and now detailed, prior theoretical and experimental work suggest that it does not occur atop and in the uppermost portion of an aqueous surface.

The surface of HNO_3 aqueous solutions has been the focus of several experimental studies. Shultz et al.[6−8,10] have studied the surface O−H infrared surface-sensitive SFG spectra of HNO_3 aqueous solutions. It was found that the surface water hydrogen (H)-bonding network was disrupted as the HNO_3 bulk concentration increased, an occurrence attributed to molecular HNO_3 approaching the surface from the bulk. The Richmond group's surface-sensitive vibrational spectroscopy results for

* To whom correspondence should be addressed. E-mail: roberto.bianco@colorado.edu.
† University of Colorado.
‡ Ecole Normale Supérieure.
§ CNRS UMR Pasteur.

10.1021/jp808533y CCC: $40.75
Published on Web 01/27/2009

N−O stretching modes of HNO_3[11] clearly show that molecular HNO_3 can exist at an aqueous surface even for solutions at a moderate HNO_3 concentration. The surface tension lowering of H_2SO_4 aqueous solutions after HNO_3 addition observed by Donaldson et al.[4] also suggests the existence of molecular HNO_3 at the air−water interface. In an infrared transmission spectroscopy study of the kinetics of dissociation of HNO_3 at an ice surface at 150 K (with monolayer or greater HNO_3 coverage) by Pursell et al.,[12] it was argued that the acid would dissociate only after diffusing 4−7 Å into the surface layer. These results, however, do not directly address the issue of present focus of an HNO_3 in a water surface at dilute concentration.

We select Car−Parrinello molecular dynamics (CPMD) to address the two questions raised at the beginning of this Introduction. While CPMD or related methods have been used to study nitric acid water clusters[30,31] and nitric acid hydrate crystals;[32] a similar methodology, Born−Oppenheimer MD, has only very recently been applied to the surface of nitric acid aqueous solutions,[3] where an HNO_3 molecule is placed on top of a water surface. Here, we use CPMD to study the acid dissociation of an HNO_3 molecule at various depths in a water surface whose corresponding HNO_3 concentration is ∼1.5 M. The occurrence of acid dissociation is connected to details of the solvation conditions and HNO_3 orientations at various depths. In addition, the key features of the solvation evolution which are necessary for this proton transfer reaction are extracted from the detailed analysis of the trajectories.

The outline of the remainder of this paper is as follows. The methodology is presented in section 2, with the results of HNO_3 acid dissociation at various depths presented and some general aspects of the trajectories discussed in section 3. In section 4, we analyze in detail the relationship between acid dissociation and the evolution of the solvation environment of HNO_3. Concluding remarks are offered in section 5.

2. Methodology

The model system involves a simulation box of dimensions $9 \times 9 \times 25$ Å^3 subject to 2D *XY* periodic boundary conditions (PBCs) containing a 14 Å thick slab (along *Z*) of 37 H_2O molecules, comprising five horizontal water layers, plus a single HNO_3 molecule, embedded inside or on top. This setup mimics low coverage conditions (<0.1 monolayer, or $1 \rightarrow 3 \times 10^{14}$ molecules/cm^2) for HNO_3 uptake in cirrus cloud particles.[14,15] The 14 Å thickness of the slab follows the inference from ref 12 that HNO_3 should dissociate at a depth ranging between 4 and 7 Å in an aqueous solution, resulting in the center of the slab being located at 7 Å, i.e., in approximately the middle third water layer of the five-layer system (by observation of the oxygens of the water molecules).

The *Z* dimension of the simulation box is larger than the thickness of the water slab to allow for surface relaxation. The width of 9 Å in the *X* and *Y* dimensions was chosen such that both HNO_3 and its conjugate base NO_3^- have enough solvation and are separated from their images by at least one H_2O molecule to prevent artificially synergetic proton transfer. In all configurations, the N images are 9 Å apart, and the direction of the O−H bond in HNO_3 is mostly not in the *XY* plane. Thus, there is no strong interaction between HNO_3 images that could artificially promote acid dissociation. Concerning the solvent-separated pairs (SSP), examination of the distances between the O of the hydronium ion and N and its nearest-neighbor images when an SSP is present, shows for all trajectories that configurations with two SSPs (with a single separating water) sharing the same H_3O^+ ion are very rare and/or very short-lived (∼20 fs). Thus, boundary effects are unlikely to artificially stabilize the products of acid dissociation.

Car−Parrinello molecular dynamics simulations were performed with the CPMD package version 3.11.1,[33] with density functional theory (DFT) in the Kohn−Sham formalism[34] used for electronic structure calculations. The electronic charge density was described by a plane-wave basis set with an average cutoff energy of 25 Ry. Energies and forces were calculated using the exchange-correlation functional of Becke, Lee, Yang, and Parr (BLYP),[35] Vanderbilt ultrasoft pseudopotentials[36] for all atoms, and the scheme of Martyna and Tuckerman[37] to decouple the slab from its images. A time step of 5 au (∼0.12 fs) was used together with a fictitious electron mass of 800 au.[76] All simulations were performed with the temperature controlled by weak coupling to a thermostat with a target temperature of 300 K. Recent CPMD simulations on the structure and dynamic properties of bulk liquid water[38] suggest that the effective temperature is ∼20% lower than the nominal temperature. We have not estimated the effective temperature associated with our current simulations; however, given the low concentration of HNO_3, we similarly assume an effective temperature of ∼240 K, falling within the 206−264 K temperature range for the upper troposphere.[39]

All initial configurations, except for the "on top" case (see below), were derived from the same bulk configuration, equilibrated at 300 K, in a procedure described below and shown in Figure 1. The initial bulk configuration was obtained by embedding an HNO_3 molecule in the center of an ice lattice of 37 waters in a $9 \times 9 \times 14$ Å^3 simulation box subject to 3D PBCs and then equilibrating for 300 ps in the NVT ensemble via classical molecular dynamics followed by a CPMD equilibration for ∼1 ps with the O−H bond of HNO_3 constrained at 0.96 Å. The equilibrated bulk configuration was then replicated around the central box using 3D PBCs. For the initial configuration of each surface case, a new $9 \times 9 \times 14$ Å^3 box was chosen such that HNO_3 was at the desired distance from the edge of the box in the $+Z$ direction. Finally, the size of the box in the *Z* direction was increased to 25 Å with the *X* and *Y* dimensions unchanged, and 2D *XY* PBCs were applied to the new box of $9 \times 9 \times 25$ Å^3 with the two surfaces in the $\pm Z$ direction exposed to the vacuum. Thus the initial configuration of the HNO_3 solvation shell was that equilibrated in the bulk minus the waters removed when HNO_3 was placed close to the interface.

Two sets of initial configurations with different initial HNO_3 orientations (cf. Figure 2) were generated. One set of seven initial configurations, labeled A1, A2, A3, A4, A5, A6, and "bulk", with the N atom, respectively, at 0, 1, 2, 3, 4, 5, and 7 Å from the $+Z$ surface (i.e., the $+Z$ edge of the initial 14-Å-high simulation box), were generated with the O−H bond in HNO_3 pointing down toward the bulk (orientation A). The other set of three initial configurations, labeled B1, B2, and B3, with the N atom, respectively, at 0, 1, and 4 Å, from the $+Z$ surface, were generated with the O−H bond in HNO_3 pointing up toward the surface (orientation B). For illustration, the initial configurations of cases A1 and B2 are shown in Figure 2. The initial configuration of the "on top" case was generated by placing the HNO_3 molecule, doubly H-bonded in orientation A (as in trajectory I of ref 3) on top of a 37 H_2O molecule sample previously equilibrated via CPMD for 2 ps. In all the 11 initial configurations, the NO_3 molecular plane is approximately perpendicular to the XY plane.

With the initial configurations generated in the procedure specified above, the surface is initially located at ±7 Å from

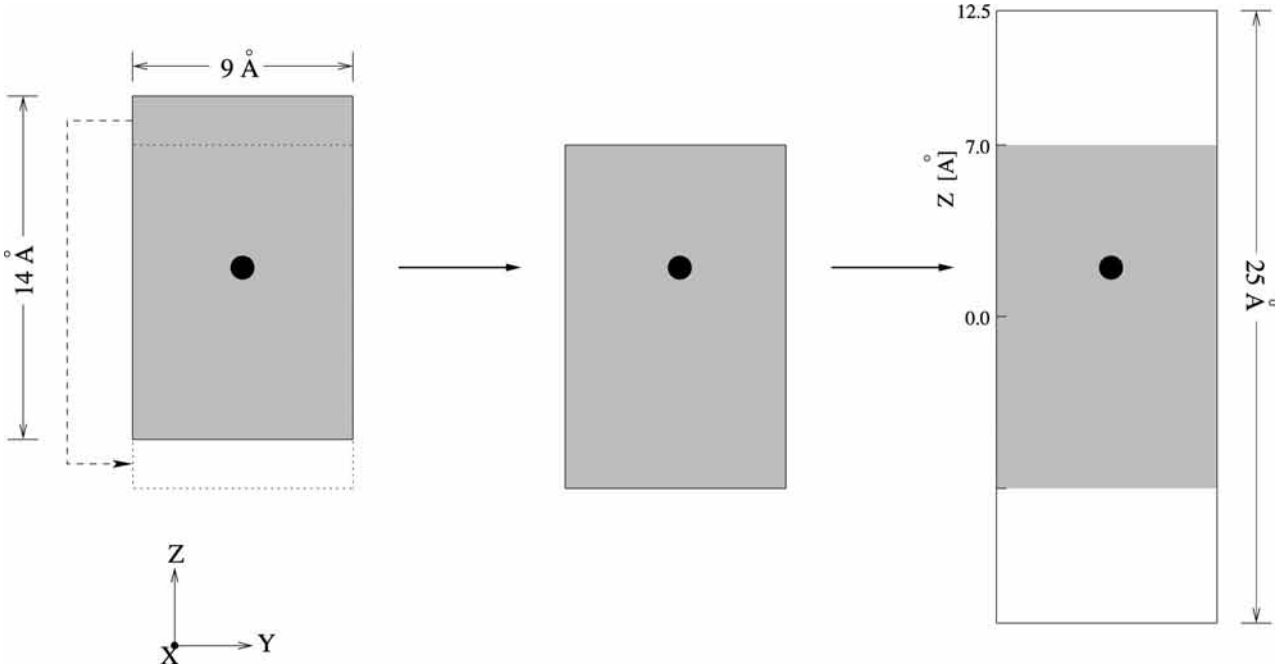

Figure 1. Generation of an initial configuration for a surface simulation from an equilibrated bulk sample simulation box. The HNO_3 molecule is represented by the black filled circle. Solid lines mark boundaries of the simulation boxes whereas dotted lines mark the sample replicated using periodic boundary conditions and shifted along the Z direction. The water slab is highlighted by the gray area.

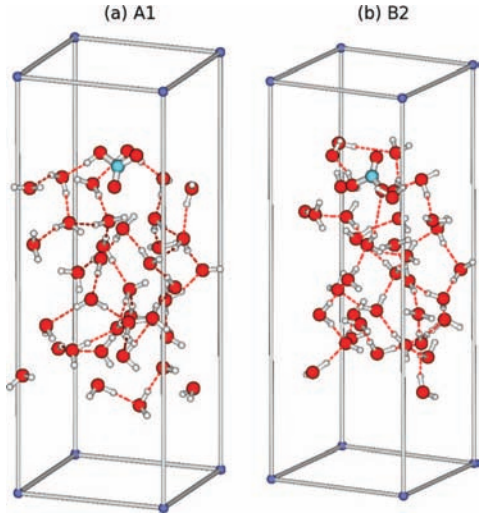

Figure 2. Initial configurations of trajectories A1 (a); with HNO_3 orientation A and B2 (b); with HNO_3 orientation B. N, cyan; O, red; H, white; H-bonds, dashed red lines.

the center of the simulation box. With the origin at the center of the simulation box, the initial z coordinates of the N atom for each of the 11 trajectories are reported in Table 1. This table also indicates that there is little vertical movement of HNO_3 or its acid dissociation product NO_3^- on the time scale of the simulations.

Starting from the initial configuration, each system was first equilibrated with the geometry of the HNO_3 molecule constrained for ~2 ps. Subsequently, the constraint was removed, and HNO_3 was allowed to dissociate in a 6-ps production run, in which the atomic position data were collected every 20 time steps (2.42 fs). After the start of the production run, the potential energy of the system usually stops decreasing sharply within 1 ps and starts oscillating.

CPMD simulations involve a classical, rather than a quantum, description of the motion of the proton. Obviously tunneling is not included, nor is the quantization of the proton bound vibrational motion. Nonetheless, some support can be given to aspects of a classical proton treatment from adiabatic proton transfer theory,[40,41] in which the bound vibrational motions of the transferring proton and the H-bond vibration are quantized. It is found[41] that a plot of the quantum averages of the proton and H-bond coordinates for a proton transfer reaction in solution is similar to a bond energy-bond order plot, which describes the proton transfer reaction path in a classical perspective.

TABLE 1: Location of the HNO_3 Nitrogen Atom[a]

trajectory	initial	avg[b]	std dev
"on top"	9.5	9.6	0.1
A1	7.0	6.8	0.1
A2	6.0	6.1	0.1
A3	5.0	5.1	0.1
A4	4.0	4.0	0.2
A5	3.0	3.2	0.2
A6	2.0	2.6	0.3
B1	7.0	7.3	0.1
B2	6.0	5.7	0.1
B3	3.0	2.5	0.2
"bulk"	0.0	0.6	0.4

[a] z coordinate of the HNO_3 nitrogen relative to the center of the simulation box, in Å. [b] The average (avg) and standard deviation (std dev) are calculated over the entire 6-ps trajectories.

3. Nitric Acid Depth-Dependent Dissociation

In this section, we present the results for HNO_3 acid dissociation, or lack thereof, at various depths and orientations. For this purpose, we decompose HNO_3 acid dissociation into two steps

$$\begin{aligned} &H_2O_b \cdots H_2O_a \cdots HO_dNO_2 \text{ (NP)} \\ &\quad \rightarrow H_2O_b \cdots H_2O_aH^+ \cdots O_dNO_2^- \text{ (CIP)} \\ &\quad \rightarrow H_2O_bH^+ \cdots HO_aH \cdots O_dNO_2^- \text{ (SSP)} \end{aligned} \qquad (2)$$

where NP denotes a neutral pair, CIP a contact ion pair, and SSP a solvent-separated ion pair. A schematic illustration of

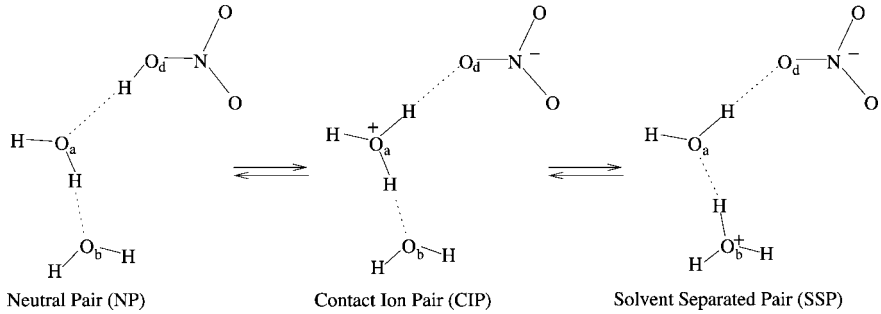

Figure 3. Schematics of double proton transfer NP→CIP→SSP for HNO_3 acid dissociation.

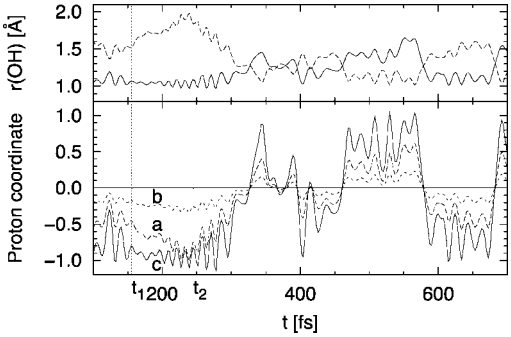

Figure 4. PT coordinate functional forms. Top panel: Trajectories of the O−H distances used to calculate the PT coordinates. Solid line, R_{O_dH}; dashed line, R_{O_aH}. Bottom panel: Trajectories of three PT coordinates. (a) Long dashed line, Q_{PT}, eq 3; (b) short dashed line, Q_{PT}', eq 4; (c) solid line, q_{PT}, eq 5. See Figure 3 for the labeling of the oxygen atoms.

the process is shown in Figure 3. Since the focus of this study is the first proton transfer step from the NP to the CIP, we first analyze, in section 3.1, each trajectory using a PT coordinate defined for this step. Section 3.2 deals with the second PT step (CIP→SSP). Section 3.3 provides an overview of the results, and comparison with previous results is given in section 3.4.

3.1. First Proton Transfer Step: NP→CIP. Before proceeding, we pause to describe the procedure used in this study to identify different species—H_2O, H_3O^+, HNO_3, and NO_3^-—and H-bonds between them. First, each H atom was assigned to the nearest O atom. Then the H_2O and H_3O^+ species were identified by those O atoms that had two or three H atoms, respectively, and NO_3^- and HNO_3 by the NO_3 moiety (N with its three nearest-neighbor O atoms) with zero or one H atom, respectively. H-bonds (O−H···O) between these species were found with a widely accepted set of criteria:[42] R(OO) < 3.5 Å, R(OH) < 2.45 Å, and ∠HOO < 30 degrees. After the species and H-bonds were identified as above, the dissociation state of nitric acid—NP, CIP, or SSP—in a configuration was readily determined. Concerning the acid dissociation reactions, the PT coordinate is customarily defined as

$$Q_{PT} = R_{O_dH} - R_{O_aH} \tag{3}$$

where R_{O_dH} and R_{O_aH} are the distances from the proton to the oxygens O_d and O_a, respectively, with labels defined in eq 2 and Figure 3. This definition is satisfactory for situations with a fixed donor−acceptor O−O distance. However, in CPMD simulations without geometry constraints, this definition is inadequate and sometimes even misleading. For instance, the plot of Q_{PT} for the $HNO_3 \cdot H_2O \rightarrow NO_3^- \cdot H_3O^+$ trajectory displayed in Figure 4, trace *a*, does not afford a consistent identification of the NP vs the CIP, since the Q_{PT} values at times t_1 and t_2 in the plot, although significantly different (−0.45 Å vs −0.74 Å), in fact correspond to situations in which HNO_3 is fully molecular with almost the same value of R_{O_dH} (1.06 Å vs 1.09 Å; see the top panel in Figure 4). This large difference mostly results from the very different R_{O_aH} values at times t_1 and t_2. A visually more appealing and convenient definition of the PT coordinate is the following

$$Q'_{PT} = \frac{R_{O_dH} - R_{O_aH}}{R_{O_dH} + R_{O_aH}} \tag{4}$$

whose plot is displayed in trace *b* of Figure 4. The effect of the denominator is to "flatten" the plot at the wings, thus more clearly highlighting the proton transfer and better reflecting the status of NP or CIP. A minor drawback of this representation is that the plot is largely contained between the values of ±0.3, instead of a more convenient set of boundaries of ±1.0. This is eliminated in the formula for q_{PT} adopted in this paper

$$q_{PT} = \frac{\Delta R_{O_dH} - \Delta R_{O_aH}}{\Delta R_{O_dH} + \Delta R_{O_aH}} \tag{5}$$

where $\Delta R_{O_dH} = R_{O_dH} - \bar{R}_{OH}(HNO_3)$ and $\Delta R_{O_aH} = R_{O_aH} - \bar{R}_{OH}(H_3O^+)$, as displayed in trace *c* of Figure 4, with $\bar{R}_{OH}(HNO_3) = 1.016$ Å and $\bar{R}_{OH}(H_3O^+) = 1.029$ Å obtained as averages from the simulations in trajectory intervals removed from PT events, where it is clear that either an NP or a CIP is present. This dimensionless PT coordinate q_{PT} lies mainly between the values −1 and +1, which correspond to an NP and a CIP, respectively. A q_{PT} value of 0 represents the situation with the proton approximately in the middle of O_d and O_a.

The PT coordinates q_{PT} of the stored configurations with either an NP or a CIP present were calculated for each trajectory and are displayed in Figure 5. The blank spaces in some of the trajectories signal the existence of either an HNO_3 without H-bonds to its acidic proton or an SSP, in which case q_{PT} is not defined. The blank space after a segment of $q_{PT} \approx +1$ represents an SSP, as in cases A1, A2, A3, A5, A6, "bulk", and B3, whereas that around a segment of $q_{PT} \approx -1$ represents HNO_3 with a non-H-bonded OH unit, as in case B1. (Further analysis of SSPs is given in section 3.2.)

The position of the HNO_3 molecule relative to the surface in each trajectory is represented by the average z coordinate of the N atom over the entire 6 ps run, with $z = 0$ assigned at the center of the simulation box, as shown in Table 1 and Figure 5. The surface in the $+Z$ direction is initially located at $z \approx 7$ Å. Because of the limited simulation time and the small sample, the calculated interfacial density profile is jagged, thus preventing us from statistically locating the surface. However, by tracking the z coordinates of the water oxygen atoms in the two outermost layers of the water slab, we found that expansion of the system during the simulations is negligible. Therefore,

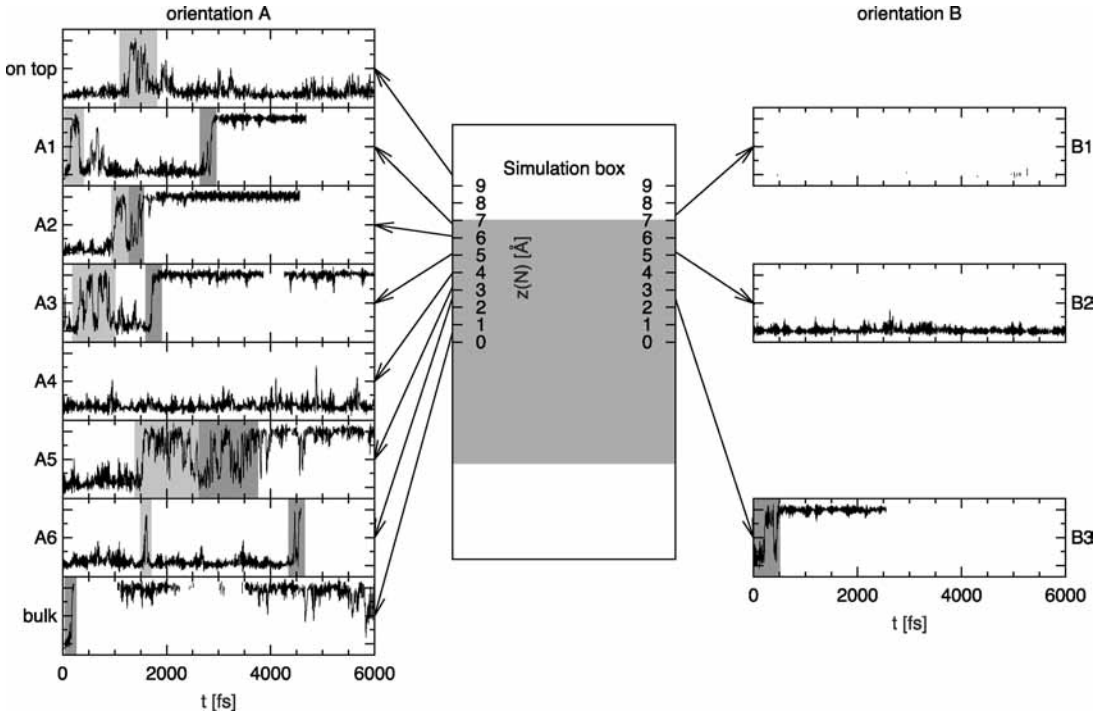

Figure 5. Summary of the simulations. Middle panel: A schematic illustration of the simulation box with the water slab highlighted in gray. The positive part of the Z axis is shown on the edges of the box. Left and right panels: Trajectories of the PT coordinate q_{PT} (eq 5) of all 11 simulations. Trajectories with the HNO_3 molecule in orientations A and B are in the left and right panels, respectively (cf. Figure 2). Each plot has an arrow pointing to the average z coordinate of the N atom in the simulation. Gray areas mark the regions selected for the analysis in section 4: dark gray for successful acid dissociation events; light gray for unsuccessful events. The y tics in each trajectory plot are -1, -0.5, 0, 0.5, and 1.

the $+Z$ surface can safely be considered as located at $z \approx 7$ Å for all trajectories.

As noted in section 2, HNO_3 and its acid dissociation product NO_3^- do not move significantly from their initial positions during the simulation period and thus do not migrate between horizontal water "layers".[43] Therefore, the water layer in which HNO_3/NO_3^- is embedded, determined by observation, will be used to refer to their position in the water slab in the ensuing discussion (see Figures 6 and 7 for snapshots of trajectories with HNO_3 orientations A and B, respectively). If we are referring to a location approximately midway between, e.g., the first and second water layers, we will denote this situation as first/second layer. If the location referred to is, e.g., somewhat closer to the second than the first layer, we will comment on this explicitly. We now discuss some general features of the trajectory results.

In the "on top" case, where the acid molecule is atop the first, surface, layer of waters (Figure 6a), HNO_3 remains molecular most of the time, with only a transient dissociation event corresponding to a short-lived CIP reverting to an NP between 1.2 and 1.6 ps (cf. Figure 5). Conversely, in the "bulk" case, where HNO_3 is located in the middle of the water slab, i.e., at the third layer (Figure 6h), acid dissociation occurs within 100 fs of the beginning of the trajectory and HNO_3 remains dissociated most of the time afterward (cf. Figure 5). These findings are consistent with the fact that HNO_3 is a strong acid in the bulk of dilute solutions at room temperature[13] and also with previous theoretical and experimental studies of HNO_3 acid dissociation on aqueous surfaces.[1,3−12]

Turning to the other trajectories with HNO_3 initially at intermediate depths, there is a mixture of HNO_3 behaviors shown in Figure 5. The general trend is that HNO_3 dissociates in the first and second surface water layers, when positioned in orientation A (O−H bond in HNO_3 pointing down toward the bulk, cf. Figure 6), except for case A4, in which HNO_3 remains molecular during the entire 6 ps period, whereas HNO_3 in orientation B (O−H bond pointing toward the surface, cf. Figure 7) remains molecular above the second layer (cases B1 and B2) until it is embedded deep into the slab below the second layer (B3). With the A4, B1, and B2 exceptions aside, this dissociation trend is consistent with chemical intuition: the degree of dissociation of an acid species is proportional to its degree of solvation. However, for all dissociated cases with HNO_3 at different depths, the timing for the dissociation varies widely, presumably due to different initial configurations, to be discussed in section 4.

Turning to the three nondissociative cases A4, B1, and B2, the latter two are fairly easily understood. In case B1, HNO_3 is half-embedded in the first surface water layer with the O−H bond pointing into the vacuum (cf. Figure 7a). As a result, the acidic proton of HNO_3 is not H-bonded to any water molecules in most of the trajectory, as indicated by the blank spaces shown in Figure 5, thus making PT impossible. Embedded more deeply in case B2, the HNO_3 molecule is located between the first and the second layers and thus succeeds in finding a water in the first layer to form an NP via the acidic proton (cf. Figure 7b). The proton-accepting water, however, is poorly solvated at this top layer with only two H-bonds, including the one with HNO_3, a solvation environment unable to stabilize the ensuing H_3O^+ ion, thus preventing HNO_3 dissociation.

The nondissociative A4 case is more complex and was examined in detail and compared to other cases, especially A3 and A5—in both of which HNO_3 dissociates—where HNO_3 is ∼1 Å above and below its position in A4, respectively. Fully embedded in the second water layer (cf. Figure 6e), the A4 NO_3 moiety is well solvated by 2−3 waters in its first hydration shell, similar to A3 and A5. In case A4, however, a striking difference was found in the orientation of the HNO_3 molecule: it rotates

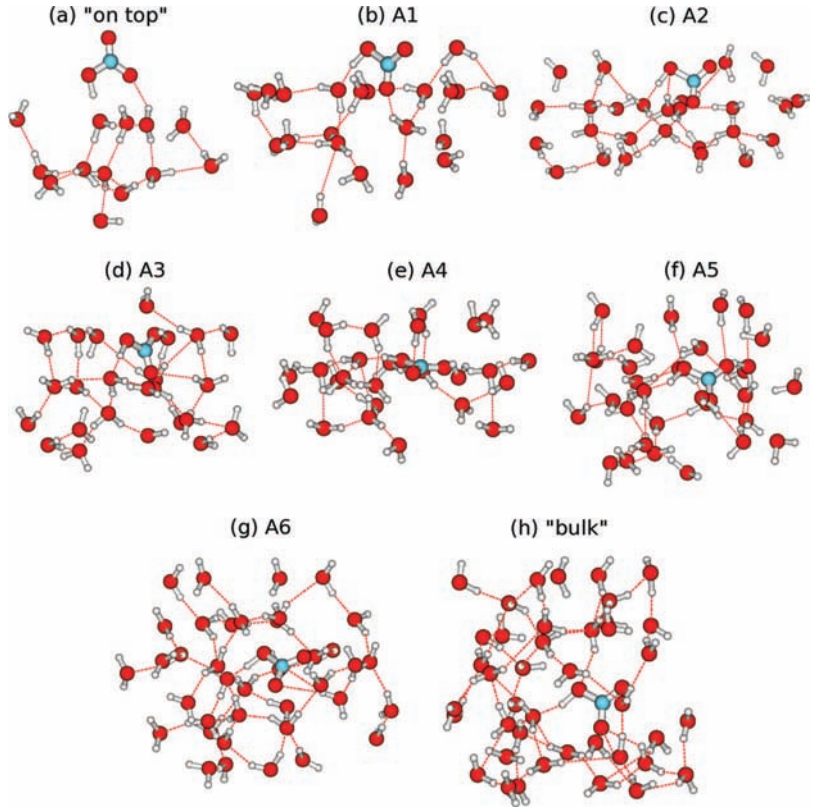

Figure 6. Snapshots of the $HNO_3 \cdot H_2O$ neutral pair in its first and second solvation shells for simulations with HNO_3 orientation A: (a) "on top" at 1685 fs; (b) A1 at 2725 fs; (c) A2 at 1294 fs; (d) A3 at 1699 fs; (e) A4 at 3205 fs; (f) A5 at 2706 fs; (g) A6 at 4412 fs; (h) "bulk" at 65 fs. Some surface waters are also included to show the embedding of HNO_3 in the water slab. The z axis is in the plane of the page pointing upward.

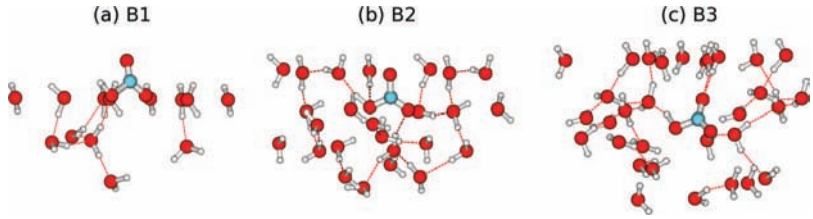

Figure 7. Snapshots of the $HNO_3 \cdot H_2O$ neutral pair in its first and second solvation shells for simulations with HNO_3 orientation B: (a) B1; (b) B2; (c) B3 at 87 fs. Some surface waters are also included to better highlight the embedding of HNO_3 in the water slab. The z axis is in the plane of the page pointing upward.

from its initial orientation, with the plane defined by the NO_3 moiety becoming nearly parallel to the XY plane (cf. Figure 6e), an occurrence absent in all the other 10 cases. After the flip, the surface waters atop the NO_3 plane were found to have been pushed aside, whereas in all the other 10 cases solvating waters are present on both sides of the NO_3 plane. Given the good solvation in the first hydration shell, this peculiar configuration of outer solvent waters would not be expected to be responsible for the lack of dissociation in A4. In fact, an explanation of this behavior requires detailed analysis of solvent motions around both the nitrate group and proton-accepting water and will be provided in section 4.

3.2. SSP and Second Proton Transfer Step (CIP→SSP). While our main focus is the NP→CIP PT, we give some discussion of SSP formation. As noted in section 2, the SSP state is signaled by blank spaces between segments of $q_{PT} \approx 1$ in Figure 5. SSPs were found in all of the seven trajectories with HNO_3 dissociated in the end of the 6-ps period. Among them, six trajectories, A1, A2, A3, A6, "bulk", and B3, were found to be in an SSP state for at least 400 fs, whereas in A5 the SSP was very short-lived (<100 fs). In trajectories A1, A2, A3, and B3, HNO_3 dissociation produces a stable CIP, which then becomes an SSP via the second proton transfer step from O_a to O_b (cf. Figure 3 for labeling), whereas in trajectories A6 and "bulk" the CIP intermediate has a much shorter lifetime before evolving into the SSP. It is very rare to find SSPs with more than two separating waters, and indeed the majority have only one water. In trajectories A2, A3, "bulk", and B3, nearly all the SSPs have one water molecule between the ions, whereas in cases A1 and A6 ~80% of the SSPs have one separating water, with the remainder having two.

3.3. Overview. Whether acid dissociation occurs or not, given a certain depth and orientation, depends on the local solvation of the NP ($HNO_3 \cdot H_2O$) species. For all trajectories with orientation A, including the "on top" case, where the O−H bond of HNO_3 points toward the bulk, the proton-accepting water of the NP is strongly H-bonded to at least two solvent waters, with the hydration of the NO_3 moiety increasing from the "on top" case to the third water layer "bulk" case. When the proton-accepting water is well solvated, as in all of the cases with orientation A, hydration of the NO_3 moiety determines acid dissociation, as illustrated by the stark differences in the "on top" case and the first layer case A1. In the "on top" case, the NO_3 moiety only forms one H-bond with a solvent water (Figure

6a), whereas in case A1 (Figure 6b), the NO_3 moiety is H-bonded to two waters. As the depth increases, more waters are H-bonded to the NO_3 moiety, and HNO_3 is found to dissociate, except for the second layer case A4, whose atypical behavior will be explained in the next section.

In the trajectories with orientation B, where the O−H bond of HNO_3 points away from the bulk, the situation is reversed compared to the A cases: the NO_3 moiety is well solvated in all three B cases, whereas the proton-accepting water is either absent or very poorly solvated (the first water layer case B1 and the first/second layer case B2) or is well solvated (the second/third layer case B3). Correspondingly, HNO_3 was found to dissociate only in case B3, where a full solvation shell around the whole NP is present. For this case, we found that hydration of the proton-accepting water is crucial: if this feature is weak, even with an NO_3 moiety well-solvated, HNO_3 does not dissociate. When the proton-accepting water is well solvated, as in all of the cases with orientation A, hydration of the NO_3 moiety determines acid dissociation, as noted above for the trajectories "on top" and A1.

3.4. Comparison with Previous Work. A comparison can be made between the results of our CPMD simulations and the ab initio MD (AIMD) simulations in ref 3. In both studies, HNO_3 is found to remain molecular when adsorbed on top of an extended water slab via two H-bonds and to dissociate readily when maximally solvated, i.e., in the third water layer "bulk" case in the present study and in the bulk simulations in ref 3. Although the HNO_3/H_2O system was simulated using different AIMD methods—CPMD in the current study and Born−Oppenheimer MD in ref 3—the qualities of the results are expected to be similar.[44] The current study, however, provides detailed information on the HNO_3 dissociation behavior at various depths in a water slab, an issue not addressed in ref 3.

In our previous theoretical study of nitric acid surface dissociation,[1] four cases in which HNO_3 was embedded in a surface-mimic water cluster with an increasing degree of hydration of the NO_3 group were studied at the HF/SBK+(d)/EFP level (HF/EFP), where the aqueous solvation was described via classical, polarizable waters of fixed internal structure (effective fragment potentials, EFP[45]) in a first attempt to understand the depth-dependent dissociation of nitric acid using computational chemistry methods. The four clusters comprise 33, 40, 45, and 50 EFP waters, respectively, solvating a variously embedded $HNO_3 \cdot (H_2O)_3$ quantum system.

Comparison of the results of the current study with those of our previous calculation[1] reveals both similarities and differences. Our "on top" case (Figure 6a) resembles case I in ref 1 in HNO_3's H-bonding and orientation, and both cases similarly indicate molecular HNO_3 atop the surface of a water slab. Cases A1, A2, and A3 in the current study resemble cases II, III, and IV in ref 1, respectively, in terms of the embedding and hydration of the NO_3 group (parts b, c, and d of Figure 6). HNO_3, however, is found to be much more prone to dissociation in the current study's surface cases than in the HF/EFP study: in cases A1, A2, and A3, HNO_3 transfers its proton to H_2O within 3 ps, and there is no sign of recombination before the end of the 6 ps simulation runs; in ref 1, the estimated reaction free energies ΔG for cases II, III, and IV were all larger than 2.6 kcal/mol at 300 K, thermodynamically disfavoring HNO_3 acid dissociation. However, since the effective temperature of the 300 K CPMD simulations in this study is estimated to be ∼240 K (cf. section 2), the current results should be compared to the HF/EFP 240 K results. Even at this lower temperature, the HF/EFP study gives a ΔG of 2.43 kcal/mol for case IV, the most solvated among the four cases, which still disfavors HNO_3 acid dissociation at aqueous surfaces, albeit to a lesser extent.

Several methodological differences between ref 1 and the current study are worth pointing out: (1) The level of electronic structure calculations differs: HF/SBK+(d) for the former and DFT-BLYP with a plane-wave basis set for the latter; (2) in the HF/EFP study, all four clusters were fully optimized at 0 K, whereas the current CPMD trajectories describe the dynamics of the system at 240 K, above configurational minima, with implications for the degree of solvation; (3) the HF/EFP study used classical, polarizable waters of fixed internal structure[45] for solvation, whereas the waters in the current CPMD study are all treated ab initio and have no structural constraints.

Both the HF/EFP and the CPMD studies have limitations. The HF/EFP study[1] predicts molecular HNO_3 at an aqueous surface. The unfavorable ΔG for acid dissociation calculated in that study, however, might be overestimated because the transition state and subsequently the products cluster were obtained from a starting point near the reactants side thus preserving the solvation environment of the reactants to some extent. On the other hand, the DFT methodology used to calculate the electronic energy in our CPMD simulations has a tendency to prefer ionic species to neutral species and underestimate proton transfer barriers.[46,47] Given the opposite directions of the most plausible estimate mistakes, the real system might resemble a situation intermediate between the two calculations.

Despite the uncertainties and disagreements in theoretical studies and the limited durations of the present CPMD simulation runs, which would not suffice to provide a statistical picture of the surface acid dissociation, we can exploit the present calculations to examine in detail the dynamics important for the HNO_3 acid dissociation proton transfers which do occur and how they vary from the bulk to the surface. This is the topic of the next section.

4. HNO_3 Acid Dissociation and Nearest-Neighbor Solvation

As discussed in section 3, HNO_3 acid dissociation involves rearrangement of solvent waters, especially those in the first solvation shell of the NP. The importance of the nearest-neighbor solvation reorganization on acid dissociation has been stressed by Ando and Hynes on HCl[48,49] and HF[50] dissociation in water. In this section, we offer a detailed analysis of this aspect on HNO_3 dissociation. After a discussion of the trajectory classification in section 4.1, the successful NP→CIP HNO_3 acid dissociation events are analyzed in section 4.2 in terms of four key features related to the hydration shell of the $HNO_3 \cdot H_2O$ NP. Unsuccessful NP→CIP trajectories are similarly analyzed in section 4.3. This is followed in section 4.4 by an analysis of special successful dissociation trajectories that produce SSPs without a stabilized CIP intermediation. After a recounting of the occurrence of Eigen (H_3O^+)[51] and Zundel ($H_5O_2^+$) cations in section 4.5, the HNO_3 dissociation at the surface and in the bulk are contrasted in section 4.6.

4.1. Classification of Trajectories. A number of acid dissociation events were identified by inspecting the q_{PT} trajectories (cf. eq 5) in Figure 5 for an increase from −1 to 1, i.e., NP→CIP. A dissociation event is considered successful if the dissociation products H_3O^+ and NO_3^- stay in the CIP state or the SSP state for more than 1.5 ps and unsuccessful if the two ions recombine shortly after the acid dissociation in less than 1.5 ps. This time interval is chosen in accordance with the experimentally measured proton hopping time in pure water of

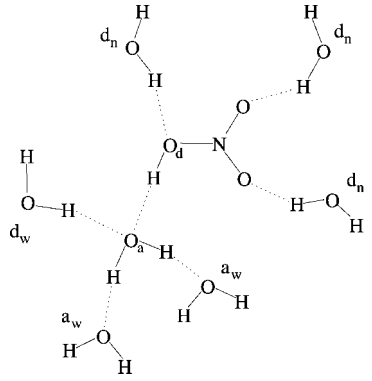

Figure 8. The neutral pair NP ($H_2O_a\cdots HO_dNO_2$) with solvent waters in its first solvation shell.

$\sim$1.5 ps.[52,77] Within this time interval, the transferring proton can vibrate for $\sim 10^3$ times in the CIP state, assuming the frequency of the H_3O^+ stretch is $\sim$2600 cm^{-1}.[2] In the ensuing discussion, successful (S) and unsuccessful (US) dissociation events in a trajectory Tr will be referred to as Tr-S and Tr-US, respectively. Seven successful and six unsuccessful events were selected using the above criteria, as shown in the light and dark gray regions in Figure 5. Among the seven successful events, two different patterns of structural evolution were observed. In the first pattern, an NP becomes a CIP and remains in this state for at least a few hundred fs before evolving into an SSP. Dissociation events A1-S, A2-S, A3-S, A5-S, and B3−S, are classified into this category. The other two events A6-S and "bulk"-S are examples of the second structural pattern, in which the dissociation products remain in the CIP state for only a few tens of fs before the H_3O^+ transfers a proton to a nearby solvent water, thus forming an SSP.

To facilitate the ensuing discussion of the solvent reorganization, labels are assigned in Figure 8 to solvent waters in the first solvation shell of the $HNO_3\cdot H_2O$ NP to distinguish their different roles. A solvent water which is the H-bond acceptor of the proton-accepting water will be referred to as type a_w, the H-bond donor to the proton-accepting water as type d_w, and the H-bond donor to an NO_3 group's oxygen (O_n) as type d_n. For each dissociation event, the solvent waters belonging to the first solvation shell of the NP/CIP, at any time along the trajectory, were tagged, and the O_d−O_a distance, the coordination number of the proton-accepting water and the ensuing H_3O^+, and the structural features of the solvent waters are selectively shown in Figure 9.

4.2. Successful Acid Dissociation: NP→CIP. By examination of the five successful acid dissociation events for this first pattern, as shown in Figure 9, several key features of the structural evolution of the reactive pair and the first solvation shell waters were observed and are summarized as follows (cf. Figure 8 for labeling):

(i) The donor−acceptor O_d−O_a distance for the HNO_3 and proton-accepting water is always less than 2.65 Å when proton transfer occurs.

(ii) The coordination number changes from 4 for the proton-accepting water in the NP to 3 for the ensuing H_3O^+ in the CIP; this change is represented as 1→0 of n_{d_w} in the third subpanel in the plots.

(iii) Either or both of the O_{a_w}−O_a distances involved in the hydration of the proton-accepting water decrease by $\sim$0.1−0.2 Å before formation of the CIP.

(iv) Solvation of the NO_3 moiety by the d_n solvent waters becomes stronger.

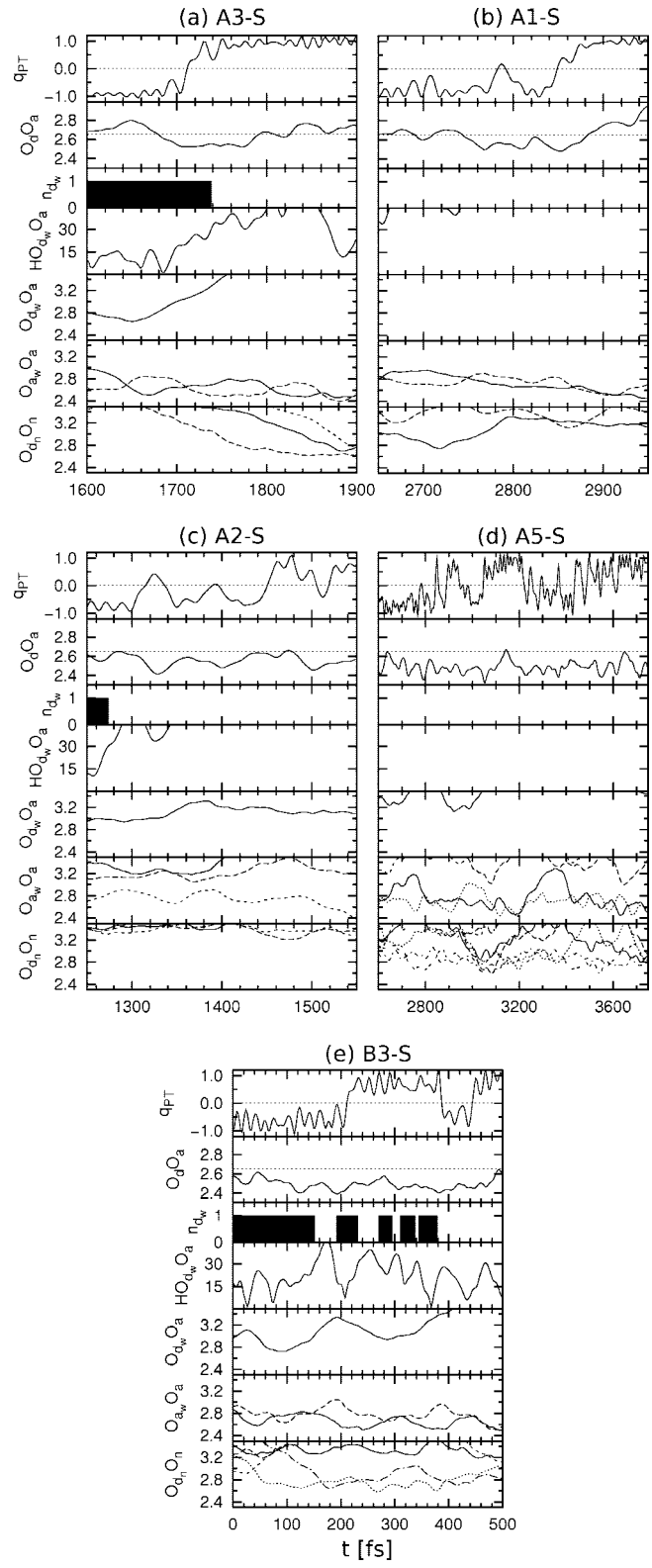

Figure 9. Successful (NP→CIP) acid dissociation events: (a) A3-S (with a stable CIP of lifetime $\tau_{CIP} \approx 2150$ fs); (b) A1-S ($\tau_{CIP} \approx 1730$ fs); (c) A2-S ($\tau_{CIP} \approx 3100$ fs); (d) A5-S ($\tau_{CIP} \approx 2400$ fs); (e) B3−S ($\tau_{CIP} \approx 2100$ fs). Note that the entire duration is not shown in each plot. Trajectory characteristics: PT coordinate q_{PT} (eq 5), O_d−O_a separation, number of H-bonds between the proton-accepting water and d_w solvent waters (n_{d_w}) (a transition of n_{d_w} from 1 to 0 corresponds to a transition of 4 to 3 for the coordination number for H_2O_a, see section 4.2), O_{d_w}−O_a distance, $HO_{d_w}O_a$ angle, O_{a_w}−O_a distance, and O_{d_n}−O_n distance, are plotted in separate subplots in each plot. Distances are in angstroms and angles in degrees.

We pause to note that the coordination number change from 4 to 3 for the proton-accepting water H_2O_a, or the reverse process, involves the breaking/forming of the H-bond between the d_w solvent water and the lone pair of O_a, assuming the presence of the other three H-bonds of H_2O_a. The change of 1→0 of n_{d_w}, i.e., the number of H-bonds between d_w solvent waters and O_a, is used instead in this study for simplicity.

The prototypical dissociation event A3-S, in which all these features are clearly detectable and come into play synergetically, is displayed in Figure 9a: q_{PT} reaches 0 at 1710 fs; $R(O_d-O_a)$ remains below 2.65 Å from 1680 to 1790 fs; the coordination number of the proton-accepting water changes from 4 to 3 at 1738 fs due to the increase of both $R(O_{d_w}-O_a)$ and the angle $\angle HO_{d_w}O_a$; the $O_{a_w}-O_a$ distances decrease; the NO_3 moiety supports two H-bonds, one appearing at 1660 fs, before the formation of the CIP, and the other at 1725 fs, both strengthening over time. The structures of the NP at 1650 fs and the CIP at 1800 fs, together with their first solvation shell waters, are shown in Figure 12, in which the configuration changes of the d_w and d_n waters are very clear. We will frequently refer to these four key features when analyzing the other cases.

These features and their roles in acid dissociation can be understood in the framework of an adiabatic proton transfer perspective.[40,41,48−50] The PT reaction between the HNO_3 and H_2O is driven by configurational changes in the surrounding environment, which modulates the shape of the proton energy surface for the transfer between O_d and O_a. A small O_d-O_a distance is necessary for a lower environmental free energy cost for the fast vibration of the transferring proton to adiabatically follow the slower rearrangement of the solvation environment. Thus the structural change i, i.e. the reduction of the O_d-O_a distance, must take place for a PT to occur. For acid dissociation, the solvation environment, especially the nearest-neighbor solvation around the proton-accepting water and HNO_3, has to rearrange to stabilize the ensuing H_3O^+ and NO_3^- ions, involving solvent motions described in features ii, iii, and iv. These three types of motions, however, differ in their importance, due to the different H-bonding strengths of H_3O^+ and NO_3^-: H_3O^+ is a hard and strong H-bonding ion, therefore a significant rearrangement of the solvent waters is necessary for $H_2O\rightarrow H_3O^+$, as shown in features ii and iii. Condition ii, the coordination number reduction from 4 to 3 for the proton-accepting water, was emphasized by Ando and Hynes[48−50] as the key solvent motion for the PT from an acid to a water and has been observed in other studies of acid dissociation in bulk[53,54] and on surfaces[55] and of an excess proton in water.[56,57] Condition iii, the strengthening of the H-bonds between the proton-accepting water and its a_w solvent waters, is also very important for the stabilization of H_3O^+.

By contrast with the preceding condition iii on H_3O^+ stabilization, condition iv deals with stabilization of the other HNO_3 dissociation product, NO_3^-. This is a weak H-bonding ion:[58] the H-bond interaction strength for nitrate−water complexes was found to be weaker than Cl^- and comparable to Br^-. In this connection, it has been found that the solvent rearrangement around the incipient anion is important for HF dissociation[59] but not so important for HCl and even less important for HBr. Thus, when the NO_3 moiety is already well solvated, as in the deeply embedded cases (e.g., the second/third layer case A6, Figure 6g), solvent reorganization around nitrate as indicated in condition iv, i.e., the increase in number and/or in strength of the H-bonds, is similarly expected to be less significant in HNO_3 dissociation and is not as important as that around the incipient H_3O^+. However, when the NO_3 moiety is poorly solvated, as in the surface cases with HNO_3 orientation A (e.g., the first layer case A1, Figure 6b), a small increase in its solvation can provide the necessary stabilization for NO_3^- and thus is expected to be significant.

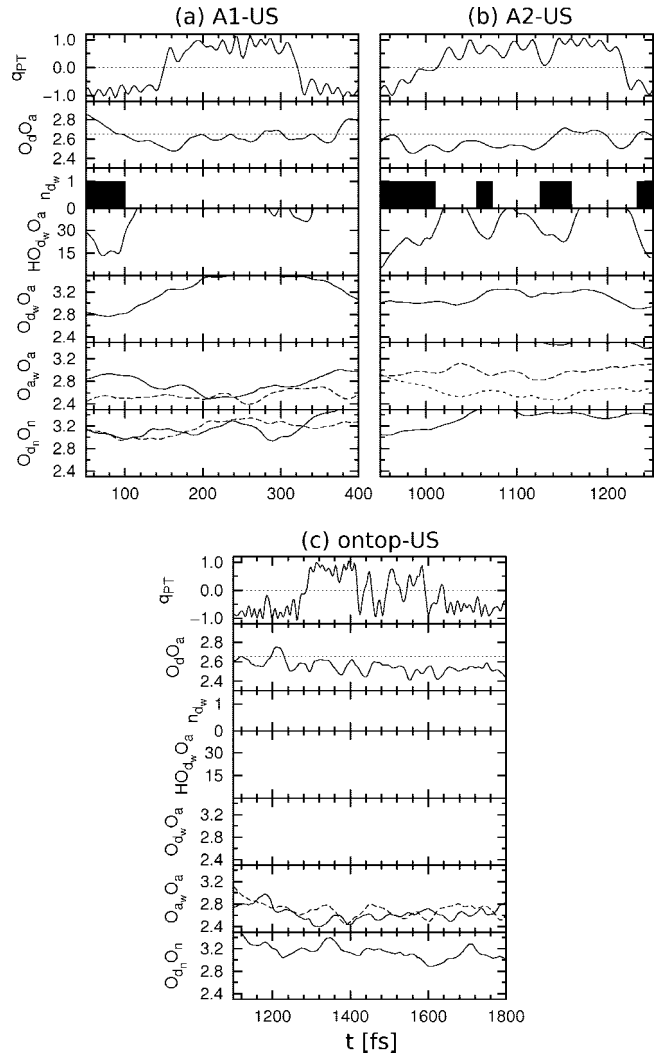

Figure 10. Unsuccessful (NP→CIP*→NP) acid dissociation events: (a) A1-US; (b) A2-US; (c) "on top"-US. See Figure 9 for Y-axis trajectory characteristics.

The timing and degree of cooperation of the four structural changes are very important for acid dissociation. In the prototypical event A3-S all four features appear to occur synergetically. In the other successful dissociation events, however, the interplay of these key changes is complex. For example, in A1-S (Figure 9b), conditions i, ii, and iii are already in place at ∼2785 fs, but the proton does not successfully transfer until 2845 fs, when the NO_3 moiety obtains two H-bonds and one of them strengthens sharply, as argued in the previous paragraph. The same pattern was observed in event A2-S (cf. Figure 9c), where the decrease of $R(O_{d_n}-O_n)$ appears to be the last condition satisfied for HNO_3 to dissociate at ∼1450 fs. Event A5-S (Figure 9d) shows a complex q_{PT} trajectory, for which the transitions between NP and CIP at 2900, 2950, 3050, and 3200−3600 fs coincide with the fluctuation of $R(O_{a_w}-O_a)$ and to a lesser extent with the fluctuation of $R(O_{d_n}-O_n)$, while conditions i and ii are satisfied in the entire interval. In event B3-S (Figure 9e) with $R(O_d-O_a)$ always below 2.65 Å and sufficient solvation of the NO_3 moiety, the acid dissociation can be attributed to the rotation of the d_w water breaking its H-bond

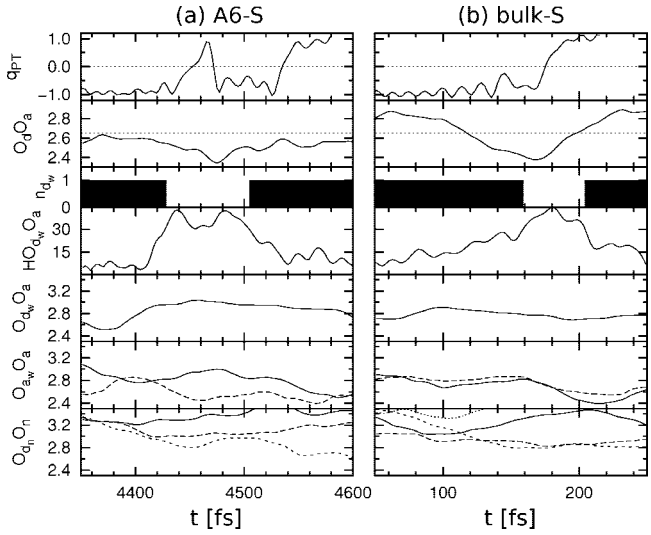

Figure 11. Successful (NP→CIP*→SSP) acid dissociation events: (a) A6-S and (b) "bulk"-S. The CIP in both events persists for ∼30 fs before transforming into an SSP. Note that the entire duration is not shown in each plot. See Figure 9 for *Y*-axis trajectory characteristics.

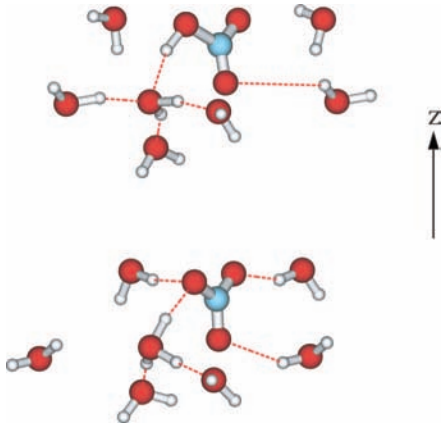

Figure 12. Simulation A3 snapshots of the NP at 1650 fs (top panel) and the CIP at 1800 fs (bottom panel) together with their first solvation shell waters.

to the lone pair of the proton-accepting water and the reduction of $R(O_{a_w}-O_a)$ around 205 fs.

Solvent reorganization around the NO_3 moiety prior to HNO_3 acid dissociation in the bulk has also been observed in a previous AIMD study of HNO_3/H_2O systems.[3] It was concluded that HNO_3 dissociation occurred in the bulk when the NO_3 moiety formed two H-bonds with $R(OH) < 2.2$ Å to nearby waters, which is consistent with our results. The more important solvation rearrangement around the proton-accepting water, however, was not reported in that study.[3]

4.3. Unsuccessful Acid Dissociation: NP→CIP*→NP. Examination of the structural changes during the unsuccessful transient dissociation events (cf. Figure 10) reveals that the four PT conditions are satisfied for the initial dissociation. The reason why these events are quickly reversed can be attributed to adverse changes in the characteristic configuration conditions ii, iii, and iv of section 4.2, even with the condition of a small O_d-O_a separation remaining satisfied. For instance, in the unsuccessful event A1-US (cf. Figure 10a), both $O_{a_w}-O_a$ distances start to increase at ∼260 fs, and thus H_3O^+ solvation is weakened, resulting in recombination at ∼320 fs, when the O_d-O_a distance decreases to ∼2.6 Å. The recombination in A2-US (cf. Figure 10b) is caused by the coordination increase from 3 to 4 for the H_3O^+, and the corresponding decrease in the solvation on this ion. For the unsuccessful event in the "on top" trajectory (cf. Figure 10c), the NO_3 moiety receives only one H-bond, insufficient to stabilize the ensuing NO_3^- ion. Although the decrease of the $O_{a_w}-O_a$ distances leads to the formation of a CIP at 1300 fs, the increase of the same distances finally causes the failure of the attempted acid dissociation.

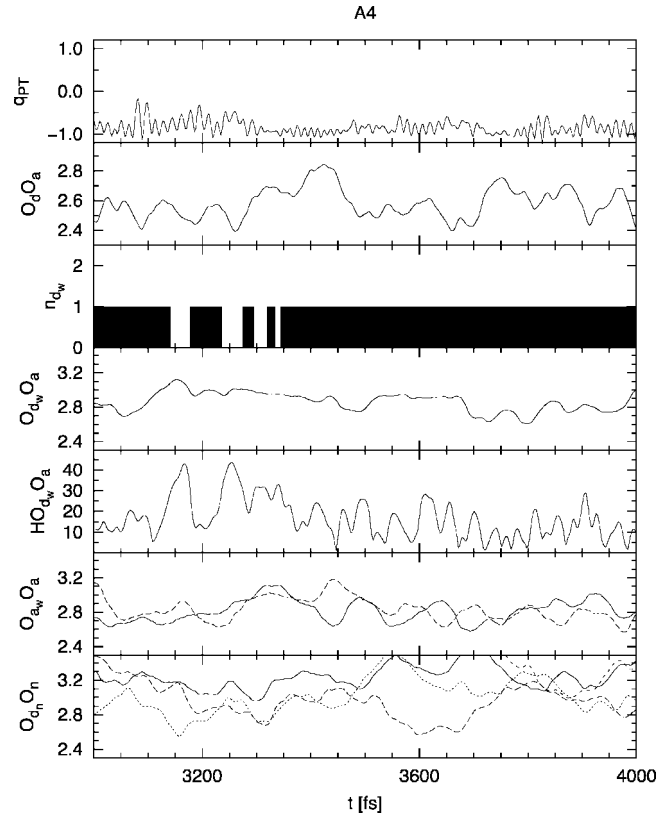

Figure 13. A typical interval for trajectory A4. See Figure 9 for *Y*-axis trajectory characteristics.

Monitoring of the nearest-neighbor solvation for trajectory A4 (cf. Figure 13 for the structural evolution in a typical trajectory interval), in which HNO_3 is fully embedded in the second water layer but fails to dissociate, shows that the proton-accepting water is tetracoordinated for almost the entire 6 ps trajectory: the strong H-bond from the d_w solvent water to the lone pair of O_a has an $O_{d_w}-O_a$ distance of ∼3.0 Å and an $HO_{d_w}O_a$ angle between 0 and 40° (see Figure 6e for a snapshot of A4). This special solvation environment around the proton-accepting water destabilizes an ensuing H_3O^+. Thus, even when the NO_3^- ion is well solvated, the CIP is still less favorable than the NP.

4.4. Successful Acid Dissociation: NP→CIP*→SSP. As mentioned earlier in this section, the two successful dissociation events A6-S and "bulk"-S display a pattern (NP→CIP*→SSP) different from the others just discussed. The CIP state in this pattern is short-lived, and the structural changes are different from the other five successful events in section 4.2 but are surprisingly similar to some of the unsuccessful events in section 4.3: the coordination number for the H_3O^+ in the CIP becomes 4 by forming an H-bond with a d_w solvent water. However, instead of transferring the proton back to the NO_3^- ion as in the unsuccessful events, the H_3O^+ in the CIP transfers another proton to an a_w solvent water to form an SSP (cf. parts a and b of Figure 11). By carefully monitoring the configurations of the solvent waters around both the NP/CIP and the a_w solvent

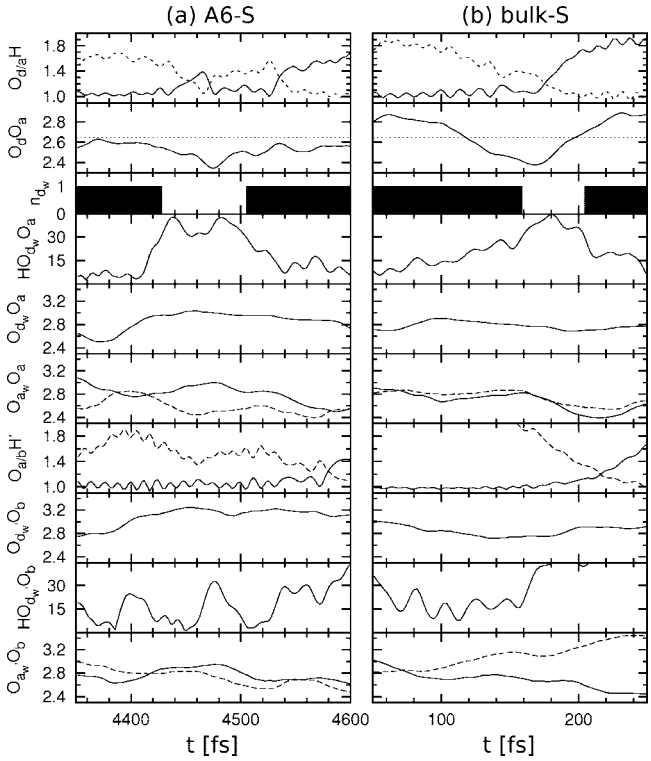

Figure 14. Structural evolution in the solvation shells of both the proton-accepting water H_2O_a and one of its a_w solvent waters H_2O_b for the successful (NP→CIP*→ SSP) acid dissociation events for (a) A6-S and (b) "bulk"-S. The CIP in both events persist for ~30 fs before becoming the SSP. Note that the entire duration is not shown in each plot. Trajectory characteristics, O_d-H/O_a-H distances, O_d-O_a separation, number of H-bonds between the proton-accepting water and d_w solvent waters (n_{d_w}), $O_{d_w}-O_a$ distance, $HO_{d_w}O_a$ angle, O_a-H'/O_b-H' distances, $O_{d_w'}-O_b$ distance, $HO_{d_w'}O_b$ angle, $O_{a_w'}-O_b$ distances, are plotted in sequence in separate panels. Distances are in angstroms and angles in degrees. See Figure 15 for labels.

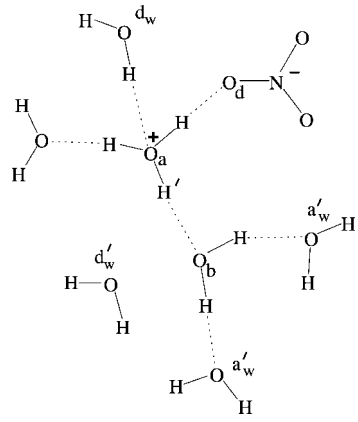

Figure 15. Schematic illustration of the short-lived CIP state and the first solvation shell of the H_3O^+ ion in the two successful acid dissociation events of the second pattern (NP→CIP*→SSP) described in section 4.4: (a) A6-S and (b) "bulk"-S. Solvent waters in the first solvation shell around H_2O_b are also shown.

water in A6-S and "bulk"-S (see Figure 14a,b for structural evolutions in A6-S and "bulk"-S, respectively, and Figure 15 for a schematic illustration of the solvation environment around the H_3O^+ in the short-lived CIP) we found that the a_w solvent water accepting the proton from the H_3O^+ in the CIP undergoes a coordination number decrease from 4 to 3, thus acquiring a solvation environment favorable to an H_3O^+ in the SSP. At the same time, the NO_3^- ion becomes sufficiently solvated (cf. parts a and b of Figure 11) to further stabilize the SSP over the NP.

TABLE 2: Fractions of Eigen vs Zundel Cations in CIP and SSP[a]

	x(Eigen)		*x*(Zundel)	
trajectory	CIP	SSP	CIP	SSP
"on top"	0.920		0.080	
A1	0.726	0.627	0.274	0.373
A2	0.660	0.575	0.340	0.425
A3	0.881	0.539	0.119	0.461
A5	0.867	0.458	0.133	0.542
A6	0.636	0.531	0.364	0.469
"bulk"	0.745	0.605	0.255	0.395
B3	0.764	0.737	0.236	0.263

[a] See section 4.5 for identification of Zundel and Eigen cations.

4.5. Eigen vs Zundel in the CIP and SSP. Whether Eigen (H_3O^+)[51,60] or Zundel ($H_5O_2^+$)[61] cations are the predominant form in acidic aqueous solutions is still an open question much discussed in the proton transport literature.[56,57,62,63] However, when the proton is near an anion in aqueous solutions, as, e.g., in a CIP, the electrostatic interaction of the anion assists in localizing the proton closer to the anion, thus favoring the Eigen cation over the Zundel.[30,64] Indeed, an Eigen cation has been found in the CIP for our previous study of HNO_3 dissociation at an aqueous interface[1] and for the CIPs associated with a number of acids in solution and elsewhere in various simulations[17,48−50,65−70] (see also recent experimental examples[64,71]). On the other hand, NO_3^- is not a particularly high charge density ion, and is not a strong H-bonding ion, being similar to bromide (Br^-).[58,72] Whatever the CIP situation is in the SSP state, the influence of the anion is screened to some degree, and Eigen cations should be less favored than in the CIP state.

To examine this issue, we calculated the fractions of Eigen vs Zundel forms in the CIP and the SSP for each trajectory using a criterion adopted by Sillanpää and Laasonen:[54] for each H_3O^+ identified in a configuration, the longest O−H bond and its associated H-bond O−H···O* were first found, and then the asymmetric H-bond coordinate $q_k = R_{O^*O}/2 - R_{OH}$ was calculated; the cation is considered to be in Eigen form if $|q_k| < 0.1$ Å and $R_{O^*O} < 2.5$ Å, and Zundel otherwise. The results of this test are summarized in Table 2, where it is seen that Eigen cations are significantly more abundant than Zundel cations in the CIPs in all trajectories. As expected, this dominance is reduced, and in one case (A5) slightly lost, in the SSPs.

4.6. Depth Dependence of Key Solvation Rearrangements. We can summarize here the most important trajectory *differences* for the surface and bulk HNO_3 acid dissociation. There are two aspects of the differing evolution of the solvation environment around the $HNO_3 \cdot H_2O$ reactive pair in the surface region and in the bulk, which we can highlight from, e.g., the successful dissociations in section 4.2.

First, the NO_3 moiety is less well solvated in the first water layer than in the third water layer "bulk" case; the H-bond from the d_w solvent water to O_a of the proton-accepting water is very likely to be present in the latter situation but absent in the former. This makes the dynamic increase of the NO_3 moiety's solvation important in the first layer cases (see the intervals 2800−2850 fs in the first layer case A1-S, Figures 9b and 6b, and 1420−1470 fs in the first/second layer, but closer to first layer, case A2-S, Figures 9c and 6c) in the sense that it is the final condition to be satisfied for the acid to dissociate. By contrast, acid dissociation is much less sensitive to this condition when HNO_3 is fully embedded (i.e., first/second layer, but closer to second layer, A3-S, second layer A5-S, second/third layer A6-S and B3-S, and third layer "bulk"-S, see Figures 9a/6d, 9d/6f, 11a/6g, 9e/7c, and 11b/6h respectively).

Second, the first water layer cases are already poised to have 3-fold coordination for the ensuing H_3O^+ product long before acid dissociation (cf. A1-S, Figures 9b and 6b, and A2-S, Figures 9c and 6c). By contrast, in the more deeply embedded and "bulk" cases, the proton transfer from HNO_3 to H_2O is generally subject to the breaking of an established d_w-O_a H-bond, i.e., the 4→3 transition in the coordination number of the proton-accepting water (cf. 1680−1740 fs in A3-S, Figures 9a and 6d, and 100−400 fs in B3−S, Figures 9e and 7c). This surface solvation feature was also observed in an earlier study of HCl acid dissociation at an ice surface[65] (see also ref 66).

5. Concluding Remarks

In this paper, we have examined the acid dissociation of a nitric acid HNO_3 molecule at different depths in an extended water slab at an effective temperature ~240 K using Car−Parrinello molecular dynamics (CPMD) simulations. Dissociation does not occur when the acid is atop the first surface layer of waters, in agreement with earlier theoretical work,[1,3] but does take place when the acid is in the third layer of the surface (the "bulk"). In between, i.e., when HNO_3 is located within the first and second surface layers, it generally dissociates, though not invariably, depending on the acid's orientation and its solvation. HNO_3 does not dissociate if either the NO_3 moiety or the proton-accepting water are not adequately solvated, to a degree depending on the depth and orientation. For these intermediate depth cases, there is some disagreement with earlier work;[1] consideration of the limitations of that work and the present suggests that HNO_3 acid dissociation may be somewhat too favored in the CPMD simulations.

Detailed examination of the trajectory dynamics indicates that the key solvent motions involved in HNO_3 acid dissociation to form an $NO_3^-\cdot H_3O^+$ contact ion pair (CIP) are: (i) a sufficiently small H-bond O−O distance between the acid and the proton-accepting water (H_2O_a); (ii) a change of the coordination of H_2O_a from 4 to 3, involving motion of the water donating an H-bond to O_a; (iii) the decrease of the O−O distances for the waters accepting H-bonds from H_2O_a; (iv) increased solvation of the NO_3 moiety by the strengthening of the H-bonds donated by solvating waters. Reversal of one or more of these conditions leads to rapid return to the $HNO_3\cdot H_2O$ neutral pair, or rapid passage to an $NO_3^-\cdot H_2O\cdot H_3O^+$ solvent-separated ion pair (SSP) without intermediate stable CIP formation. The relative importance of these conditions differs in the bulk compared to the surface regions. Finally, Eigen cation (H_3O^+) occurrence strongly dominates over Zundel cation ($H_5O_2^+$) in the CIP, with this dominance reduced in the SSP.

We have not described in any detail in the present work the transition of a stable CIP to an SSP, which is important in the ionic distribution in the aqueous surface region. This will be discussed elsewhere.

Acknowledgment. This work was supported in part by NSF Grants CHE-0417570 and CHE-0750477 and by the National Center for Supercomputing Applications under TG-CHE070039 and TG-CHE070033N and utilized the systems TUNGSTEN and ABE.

References and Notes

(1) Bianco, R.; Wang, S.; Hynes, J. T. *J. Phys. Chem. A* **2007**, *111*, 11033.
(2) Bianco, R.; Wang, S.; Hynes, J. T. *J. Phys. Chem. A* **2008**, *112*, 9467.
(3) Shamay, E. S.; Buch, V.; Parrinello, M.; Richmond, G. L. *J. Am. Chem. Soc.* **2007**, *129*, 12910.
(4) Donaldson, D. J.; Anderson, D. *Geophys. Res. Lett.* **1999**, *26*, 3625.
(5) Clifford, D.; Bartels-Rausch, T.; Donaldson, D. J. *Phys. Chem. Chem. Phys.* **2007**, *9*, 1362.
(6) Schnitzer, C.; Baldelli, S.; Campbell, D. J.; Shultz, M. J. *J. Phys. Chem. A* **1999**, *103*, 6383.
(7) Shultz, M. J.; Schnitzer, C.; Simonelli, D.; Baldelli, S. *Int. Rev. Phys. Chem.* **2000**, *19*, 123.
(8) Schnitzer, C.; Baldelli, S.; Shultz, M. J. *J. Phys. Chem. B* **2000**, *104*, 585.
(9) Yang, H.; Finlayson-Pitts, B. J. *J. Phys. Chem. A* **2001**, *105*, 1890.
(10) Shultz, M. J.; Baldelli, S.; Schnitzer, C.; Simonelli, D. *J. Phys. Chem. B* **2002**, *106*, 5313.
(11) Soule, M. C. K.; Blower, P. G.; Richmond, G. L. *J. Phys. Chem. A* **2007**, *111*, 3349.
(12) Pursell, C. J.; Everest, M. A.; Falgout, M. E.; Sanchez, D. D. *J. Phys. Chem. A* **2002**, *106*, 7764.
(13) Oxtoby, D. W.; Nachtrieb, N. H. *Principles of Modern Chemistry*, 2nd ed.; Saunders: Philadelphia, 1990.
(14) Abbatt, J. P. D. *Geophys. Res. Lett.* **1997**, *24*, 1479.
(15) Zondlo, M. A.; Barone, S. B.; Tolbert, M. A. *Geophys. Res. Lett.* **1997**, *24*, 1391.
(16) Solomon, S. *Rev. Geophysics* **1999**, *37*, 275.
(17) Bianco, R.; Hynes, J. T. *J. Phys. Chem. A* **1999**, *103*, 3797.
(18) (a) Rivera-Figueroa, A. M.; Sumner, A. L.; Finlayson-Pitts, B. J. *Environ. Sci. Technol.* **2003**, *37*, 548. (b) Mochida, M.; Finlayson-Pitts, B. J. *J. Phys. Chem. A* **2000**, *104*, 9705. (c) Saliba, N. A.; Yang, H.; Finlayson-Pitts, B. J. *J. Phys. Chem. A* **2001**, *105*, 10339.
(19) (a) Guimbaud, C.; Arens, F.; Gutzwiller, L.; Gäggeler, H. W.; Ammann, M. *Atmos. Chem. Phys.* **2002**, *2*, 249. (b) Davies, J. A.; Cox, R. A. *J. Phys. Chem. A* **1998**, *102*, 7631. (c) Beichert, P.; Finlayson-Pitts, B. J. *J. Phys. Chem.* **1996**, *100*, 15218. (d) Ghosal, S.; Hemminger, J. C. *J. Phys. Chem. B* **2004**, *108*, 14102.
(20) Lawrence, M. G.; Crutzen, P. J. *Tellus* **1998**, *50B*, 263.
(21) Solomon, S.; Borrmann, S.; Garcia, R. R.; Portmann, R.; Thomason, L.; Poole, L. R.; Winker, D.; McCormick, M. P. *J. Geophys. Res.* **1997**, *102*, 21411.
(22) Borrmann, S.; Solomon, S.; Dye, J. E.; Luo, B. P. *Geophys. Res. Lett.* **1996**, *23*, 2133.
(23) Meier, A.; Hendricks, J. *J. Geophys. Res. Atmos.* **2002**, *107*, 4696.
(24) Zondlo, M. A.; Hudson, P. K.; Prenni, A. P.; Tolbert, M. A. *Annu. Rev. Phys. Chem.* **2000**, *51*, 473.
(25) Hudson, P. K.; Shilling, J. E.; Tolbert, M. A.; Toon, O. B. *J. Phys. Chem. A* **2002**, *106*, 9874.
(26) (a) Ramazan, K. A.; Wingen, L. M.; Miller, Y.; Chaban, G. M.; Gerber, R. B.; Xantheas, S. S.; Finlayson-Pitts, B. J. *J. Phys. Chem. A* **2006**, *110*, 6886. (b) Goodman, A. L.; Bernard, E. T.; Grassian, V. H. *J. Phys. Chem. A* **2001**, *105*, 6443.
(27) Meilinger, S. K.; Kärcher, B.; Peter, Th. *Atmos. Chem. Phys.* **2005**, *5*, 533.
(28) Young, T. F.; Maranville, L. F.; Smith, H. M. *Raman Spectral Investigations of Ionic Equilibria in Solutions of Strong Electrolytes*; Hamer, W. J., Ed.; Wiley and Sons: New York, 1959; pp 38−48.
(29) Minogue, N.; Riordan, E.; Sodeau, J. R. *J. Phys. Chem. A* **2003**, *107*, 4436.
(30) Miller, Y.; Gerber, R. B. *Phys. Chem. Chem. Phys.* **2008**, *10*, 1091.
(31) Elola, M. D.; Marceca, E. J.; Laria, D.; Estrin, D. A. *Chem. Phys. Lett.* **2000**, *326*, 509.
(32) (a) Tóth, G. *J. Phys. Chem. A* **1997**, *101*, 8871. (b) Sullivan, D. M.; Bagchi, K.; Tuckerman, M. E.; Klein, M. L. *J. Phys. Chem. A* **1999**, *103*, 8678.
(33) CPMD, Copyright IBM Corp 1990−2006, Copyright MPI für Festkörperforschung Stuttgart, 1997−2001.
(34) (a) Hohenberg, P.; Kohn, W. *Phys. Rev.* **1964**, *136*, B864. (b) Kohn, W.; Sham, L. J. *Phys. Rev.* **1965**, *140*, A1133.
(35) (a) Lee, C. T.; Yang, W.; Parr, R. G. *Phys. Rev. B* **1988**, *37*, 785. (b) Becke, A. D. *Phys. Rev. A* **1988**, *38*, 3098. (c) Miehlich, B.; Savin, A.; Stoll, H.; Preuss, H. *Chem. Phys. Lett.* **1989**, *157*, 200.
(36) (a) Vanderbilt, D. *Phys. Rev. B* **1990**, *41*, 5048. (b) Laasonen, K.; Car, R.; Lee, C.; Vanderbilt, D. *Phys. Rev. B* **1991**, *43*, 6796. (c) Laasonen, K.; Pasquarello, A.; Lee, C.; Car, R.; Vanderbilt, D. *Phys. Rev. B* **1993**, *47*, 10142.
(37) Martyna, G. J.; Tuckerman, M. E. *J. Chem. Phys.* **1999**, *110*, 2810.
(38) (a) Fernández-Serra, M. V.; Artacho, E. *J. Chem. Phys.* **2004**, *121*, 11136. (b) Schwegler, E.; Grossman, J. C.; Gygi, F.; Galli, G. *J. Chem. Phys.* **2004**, *121*, 5400. (c) Lee, H.-S.; Tuckerman, M. E. *J. Chem. Phys.* **2007**, *126*, 164501.
(39) Evans, K. D.; Melfi, S. H.; Ferrare, R. A.; Whiteman, D. N. *Appl. Opt.* **1997**, *36*, 2594.
(40) Kiefer, P. M.; Hynes, J. T. *J. Phys. Chem. A* **2002**, *106*, 1834.
(41) Kiefer, P. M.; Hynes, J. T. *J. Phys. Chem. A* **2002**, *106*, 1850.
(42) Laage, D.; Hynes, J. T. *Proc. Natl. Acad. Sci. U.S.A.* **2007**, *104*, 11167.

(43) This lack of vertical interchange of, e.g., NO_3^- on a 6-ps time scale is not surprising. For the NO_3^- diffusion constant at ~240 K in water, the estimated activation energy is ~12 kcal/mol.[73] In addition to the electrostatically attractive impact of the nearby presence of an H_3O^+ in a CIP or an SSP, this indicates that the present study does not contribute to the question of any preference (or lack thereof) of an NO_3^- anion for the water surface.[74,75]

(44) Kuo, I.-F. W.; Mundy, C. J.; McGrath, M. J.; Siepmann, J. I.; VandeVondele, J.; Sprik, M.; Hutter, J.; Chen, B.; Klein, M. L.; Mohamed, F.; Krack, M.; Parrinello, M. *J. Phys. Chem. B* **2004**, *108*, 12990.

(45) (a) Day, P. N.; Jensen, J. H.; Gordon, M. S.; Webb, S. P.; Stevens, W. J.; Krauss, M.; Garmer, D.; Basch, H.; Cohen, D. *J. Chem. Phys.* **1996**, *105*, 1968. (b) Chen, W.; Gordon, M. S. *J. Chem. Phys.* **1996**, *105*, 11081.

(46) Smith, A.; Vincent, M. A.; Hillier, I. H. *J. Phys. Chem. A* **1999**, *103*, 1132.

(47) (a) Barone, V.; Orlandini, L.; Adamo, C. *Chem. Phys. Lett.* **1994**, *231*, 295. (b) Sadhukhan, S.; Munoz, D.; Adamo, C.; Scuseria, G. E. *Chem. Phys. Lett.* **1999**, *306*, 83. (c) Barone, V.; Adamo, C. *J. Chem. Phys.* **1996**, *105*, 11007. (d) Mijoule, C.; Latajka, Z.; Borgis, D. *Chem. Phys. Lett.* **1993**, *208*, 364.

(48) Ando, K.; Hynes, J. T. *J. Mol. Liq.* **1995**, *64*, 25.

(49) Ando, K.; Hynes, J. T. *J. Phys. Chem. B* **1997**, *101*, 10464.

(50) Ando, K.; Hynes, J. T. *J. Phys. Chem. A* **1999**, *103*, 10398.

(51) Here we are using the term "Eigen" for the hydronium ion H_3O^+ rather then the larger hydrated species $H_3O^+(H_2O)_3$ species often so termed.

(52) Meiboom, S. *J. Chem. Phys.* **1961**, *34*, 375.

(53) Laasonen, K.; Klein, M. L. *Mol. Phys.* **1996**, *88*, 135.

(54) Sillanpää, A. J.; Laasonen, K. *Phys. Chem. Chem. Phys.* **2004**, *6*, 555.

(55) (a) Buch, V.; Sadlej, J.; Aytemiz-Uras, N.; Devlin, J. P. *J. Phys. Chem. A* **2002**, *106*, 9374. (b) Devlin, J. P.; Uras, N.; Sadlej, J.; Buch, V. *Nature* **2002**, *417*, 269. (c) Mantz, Y. A.; Geiger, F. M.; Molina, L. T.; Molina, M. J.; Trout, B. L. *Chem. Phys. Lett.* **2001**, *348*, 285.

(56) (a) For recent reviews, see: Marx, D. *Chem. Phys. Chem* **2006**, *7*, 1848. (b) Voth, G. A. *Acc. Chem. Res.* **2006**, *39*, 143.

(57) (a) Tuckerman, M.; Laasonen, K.; Sprik, M.; Parrinello, M. *J. Phys. Chem.* **1995**, *99*, 5749. (b) Marx, D.; Tuckerman, M. E.; Hutter, J.; Parrinello, M. *Nature* **1999**, *397*, 601. (c) Geissler, P. L.; Dellago, C.; Chandler, D.; Hutter, J.; Parrinello, M. *Science* **2001**, *291*, 2121. (d) Tuckerman, M.; Laasonen, K.; Sprik, M.; Parrinello, M. *J. Chem. Phys.* **1995**, *103*, 150. (e) Schmitt, U. W.; Voth, G. A. *J. Chem. Phys.* **1999**, *111*, 9361. (f) Schmitt, U. W.; Voth, G. A. *J. Phys. Chem. B* **1998**, *102*, 5547. (g) Vuilleumier, R.; Borgis, D. *J. Phys. Chem. B* **1998**, *102*, 4261. (h) Vuilleumier, R.; Borgis, D. *J. Chem. Phys.* **1999**, *111*, 4251.

(58) Ramesh, S. G.; Re, S.; Hynes, J. T. *J. Phys. Chem. A* **2008**, *112*, 3391.

(59) Laage, D.; Kiefer, P.; Marquetand, P.; Hynes, J. T. Unpublished.

(60) (a) Wicke, E.; Eigen, M.; Ackermann, Th. *Z. Phys. Chem.* **1954**, *1*, 340. (b) Eigen, M. *Angew. Chem., Int. Ed. Engl.* **1964**, *3*, 1.

(61) (a) Zundel, G.; Metzger, H. *Z. Phys. Chem.* **1968**, *58*, 225. (b) Zundel, G. In *The Hydrogen Bond Recent Developments in Theory and Experiments. II. Structure and Spectroscopy*; Schuster, P., Zundel, G., Sandorfy, C., Eds.; North-Holland: Amsterdam, 1976; pp 683.

(62) Asthagiri, D.; Pratt, L. R.; Kress, J. D. *Proc. Natl. Acad. Sci. U.S.A.* **2005**, *102*, 6704.

(63) Headrick, J. M.; Diken, E. G.; Walters, R. S.; Hammer, N. I.; Christie, R. A.; Cui, J.; Myshakin, E. M.; Duncan, M. A.; Johnson, M. A.; Jordan, K. D. *Science* **2005**, *308*, 1765.

(64) Mohammed, O. F.; Pines, D.; Dreyer, J.; Pines, E.; Nibbering, E. T. J. *Science* **2005**, *310*, 83.

(65) (a) Gertner, B. J.; Hynes, J. T. *Science* **1996**, *271*, 1563. (b) Gertner, B. J.; Hynes, J. T. *Faraday. Discuss.* **1998**, *110*, 301.

(66) Swanson, J. M. J.; Maupin, C. M.; Chen, H.; Petersen, M. K.; Xu, J.; Wu, Y.; Voth, G. A. *J. Phys. Chem. B* **2007**, *111*, 4300.

(67) Al-Halabi, A.; Bianco, R.; Hynes, J. T. *J. Phys. Chem. A* **2002**, *106*, 7639.

(68) Bianco, R.; Hynes, J. T. *Theor. Chem. Acc.* **2004**, *111*, 182.

(69) Bianco, R.; Wang, S.; Hynes, J. T. *J. Phys. Chem. B* **2005**, *109*, 21313.

(70) Bianco, R.; Hynes, J. T. *Acc. Chem. Res.* **2006**, *39*, 159.

(71) Rini, M.; Magnes, B.-Z.; Pines, E.; Nibbering, E. T. J. *Science* **2003**, *301*, 349.

(72) $Br^- \cdot H_3O^+$ CIP was found in ref 67, but there was insufficient hydration to allow possibility of Zundel cation formation.

(73) Thibert, E.; Dominé, F. *J. Phys. Chem. B* **1998**, *102*, 4432.

(74) Salvador, P.; Curtis, J. E.; Tobias, D. J.; Jungwirth, P. *Phys. Chem. Chem. Phys.* **2003**, *5*, 3752.

(75) Dang, L. X.; Chang, T. M.; Roeselova, M.; Garrett, B. C.; Tobias, D. J. *J. Chem. Phys.* **2006**, *124*, 066101.

(76) For a recent review on CPMD simulation protocols for interface systems, see: Mundy, C. J.; Kuo, I.-F. W. *Chem. Rev.* **2006**, *106*, 1282.

(77) The proton hopping time for surface water should be somewhat different from that for bulk water due to the different solvation dynamics associated with the density variation. It is, however, difficult to estimate this effect. On one hand, the weaker and longer H-bonds between the surface waters, as reflected by the smaller water density in the surface region, should result in faster and larger solvation fluctuation, thus promoting proton hopping. On the other hand, an H_3O^+ ion at the surface might have a longer lifetime due to the decreased possibility of the H-bond formation to the oxygen's lone pair. However, the influence of the different proton hopping time at the surface on our results and conclusions is not expected to be significant. Although a different set of successful acid dissociation events would be selected if a different proton hopping time were used, our analysis has shown that the four key structural features for proton transfer are observed in both successful and unsuccessful events.

JP808533Y